

Thermal Transport Dynamics in Active Heat Transfer Fluids (AHTF)

W. Peng¹, J.L. Moran², P. Keblinski¹

1 – Department of Materials Science and Engineering, Rensselaer Polytechnic Institute, Troy, NY

2 – Department of Mechanical Engineering, George Mason University, Fairfax, VA

Abstract

We present results of molecular dynamics (MD) calculations of the effective thermal conductivity of nanofluids containing self-propelled nanoparticles. The translational and rotational dynamics observed in the simulations follow the behavior expected from the standard theoretical analysis of Brownian and self-propelled nanoparticles. The superposition of self-propulsion and rotational Brownian motion causes the behavior of the self-propelled nanoparticles to resemble Brownian diffusion at long times, with an effective coefficient that is larger than the standard Brownian value by a factor of several thousand. As a result of the enhanced diffusion (and the enhanced convective mixing resulting from the motion), we observe a discriminable increase of the effective thermal conductivity of the solution. While the increases we observe are in the range of several percent, they are significant considering that, without propulsion, the nanofluid thermal conductivity is essentially the same as that of the base fluid. Our results constitute a proof of concept that self-propelled particles have the potential to enhance thermal conductivity of the liquid in which they are immersed, an idea that could ultimately be implemented in a broad variety of cooling applications.

1. Introduction

Heat Transfer Fluids and Nanofluids

Heat transfer fluids (HTF) are important components of many engineering systems in which materials or devices need to be cooled, heated, or kept within a certain temperature range. HTF absorb, transport, and expel heat in numerous applications such as solid-state lighting, automobile thermal management (e.g. brake fluid), high-power radio-frequency (RF) devices, electricity generation, and microelectronics cooling, among others. Many of these technologies face fundamental performance limits that, in many cases, are determined by the rate of waste heat removal. The efficacy of HTF, and thus the performance of these devices, depend primarily on flow conditions, flow geometry, and fluid properties such as thermal conductivity, viscosity, and specific heat. Recent efforts have been especially devoted to increasing the thermal conductivity of liquids.

In the 1990s, Choi and Eastman introduced the concept of *nanofluids*, which are colloidal suspensions of nanoparticles in liquids¹. Since the nanoparticle materials are typically highly thermally conductive, the nanoparticle suspension usually exhibits a higher thermal conductivity than the liquid alone. Soon after nanofluids were introduced, several unexpected findings were reported regarding their thermal properties. These included (1) thermal conductivity enhancements exceeding those predicted by classical theories, such as the effective-medium theory formulated by Maxwell in the 1880s²; (2) a nonlinear dependence of thermal conductivity enhancement provided by nanoparticles on nanoparticle volume fraction; (3) a dependence of thermal conductivity enhancement on nanoparticle size and shape; (4) a dependence of thermal conductivity enhancement on liquid temperature.

The first observation—anomalous thermal conductivity enhancement—received special attention, and many theories were proposed to explain it. For example, it was postulated that “micro-convection” generated by the nanoparticles’ Brownian motion could contribute an additional mode of heat transfer enhancement, which might potentially account for the anomalous measurements. However, this hypothesis is implausible considering that the nanoparticle diffusivity is generally orders of magnitude smaller than the thermal diffusivity of the base liquid. The latter observation is consistent with molecular dynamics (MD) simulations of thermal transport in nanofluids^{3,4}, as well as carefully-executed experiments on nanofluids with well-dispersed nanoparticles^{5,6}. Brownian-motion-induced micro-convection is now understood to play a negligible role in heat transport through nanofluids⁴. In 2009, researchers from 34 organizations worldwide carefully measured the thermal conductivity of various nanofluids, using consistent and well-established experimental techniques; their main finding was that the effective-medium theory formulated by Maxwell² and generalized by Nan et al.⁷, which does not include micro-convection effects, successfully predicted the thermal conductivity of the nanofluids tested to within experimental uncertainty, suggesting that no anomalous enhancement of thermal conductivity was detected in these nanofluids⁸.

Most of the anomalous measurements of nanofluid thermal conductivity are now understood to originate either from inconsistent measurement techniques and conditions or from nanoparticle agglomeration. The extent of agglomeration in nanofluids can differ depending on the synthesis and dispersion conditions, and it can also change with time. In this context, large thermal conductivity enhancements can be attributed the formation of sparse and fractal nanoparticle agglomerates that can provide an interconnected conductive path for heat transport. However, such agglomerates tend to cause a concomitant increase in the fluid’s viscosity. In many cases, the negative effects associated with the viscosity increase (e.g. increased pumping power requirements) outweigh the benefits from the increase in thermal conductivity. The heat transfer enhancement potential of traditional nanofluids is thus limited. Nevertheless, as devices are further miniaturized, and power dissipation requirements simultaneously rise, the need for high-performance heat transfer fluids continues to increase rapidly.

Active Colloids: Self-Propelling Colloidal Particles

In the past 15 years there has been significant interest in *active colloids*, also known as *synthetic microswimmers*, which are colloidal particles that harvest energy from their surroundings and propel themselves through liquids, usually an aqueous solution. They accomplish this feat through a variety of mechanisms. Synthetic active colloids range in size from $\sim 30 \text{ nm}^9$ to $\sim 30 \text{ microns}^{10}$ and obtain energy for their propulsion from a variety of sources, such as chemical fuels, ultraviolet light, electric or magnetic fields, or ultrasound. They can perform potentially useful micro-scale tasks, such as towing cargo more than 10 times their size and moving in user-guided patterns (e.g. under magnetic fields)¹¹. These capabilities suggest potential applications in medicine such as targeted drug delivery¹² or precision surgery, environmental remediation¹³, and self-assembly of functional microstructures¹⁴, as detailed in several reviews (an accessible overview to the general field of self-propelled colloids, aimed at newcomers, can be found in ref. ¹⁵).

As they move, both natural and synthetic microswimmers agitate the fluid around them, causing disturbance flows in their vicinity. Microswimmers are often classified as “pushers” or “pullers” depending on the qualitative nature of these disturbance flows, which in turn depends on where specifically the microswimmer generates the force responsible for its propulsion. It is common to model self-propelled microswimmers as a point-force dipole, as this turns out to be the leading-order contribution in the multipole expansion for the velocity field. This is represented mathematically by the stresslet tensor, defined as $\mathbf{S} = \sigma_0 \mathbf{r}\mathbf{r}$ where \mathbf{S} is the symmetric part of the first moment of the force and \mathbf{r} is the instantaneous direction of motion. For example, the bacteria *Escherichia coli* and *Bacillus subtilis* move by deforming flagella behind their bodies; the flagella thus “push” the organisms through the fluid; these organisms are thus known as *pushers*, and their stresslet coefficient is negative: $\sigma_0 < 0$ ¹⁶. Other organisms, such as the marine alga *Chlamydomonas reinhardtii*, are known as “pullers” because they propel themselves from the front ($\sigma_0 > 0$); *C. reinhardtii* does so by waving two flagella at the front of its body in a breaststroke-like fashion¹⁷.

Pushers and pullers affect the rheological and transport properties of the surrounding fluid in different ways. Theoretical and experimental studies establish that while pullers *increase* the viscosity relative to the solvent alone¹⁸, pushers have the opposite effect: pusher suspensions show a *decrease* in viscosity compared to the liquids alone¹⁹. Furthermore, in several studies pusher microorganisms have been experimentally shown to generate meso-scale convective flows and associated enhancements in fluid mixing. Wu and Libchaber first reported that motile *Escherichia coli* bacteria enhanced the diffusion of tracer particles in a quasi-two-dimensional soap film²⁰, and a similar result was later reported in a microfluidic device²¹. If the swimmer volume fraction exceeds a certain threshold, bacterial suspensions exhibit chaotic convective motions termed “bacterial turbulence”²². In some cases, the microswimmer-associated viscosity reduction has been significant enough that the viscosity apparently vanishes, and the resulting bacterial suspensions can behave as superfluids¹⁹. Preliminary numerical studies establish that hydrodynamic interactions among pusher microswimmers lead to coherent vortex motion²³, and simulations of self-propelled rods show significant mixing enhancement compared to pullers and non-swimming particles when the volume fraction of rods exceeds a certain threshold²⁴. Although there are relatively few experimental studies that examine the collective mixing enhancement of artificial particles, Ebbens’ group at Sheffield recently showed that colloidal microspheres isotropically coated in platinum induce bulk convective flows in aqueous hydrogen peroxide solutions²⁵, although it is unclear whether the mechanism is similar to that seen in pusher bacterial suspensions.

In summary, there is a precedent for microswimmers (natural or synthetic) to enhance mixing in liquids. However, the ability of *artificial microswimmers* to enhance the transport of *thermal energy* has not been explored in detail. To our knowledge, the only previous study in this vein is that of El Hasadi and Crapper²⁶, who formulated an analytical and numerical model of “self-propelled nanofluids” and predicted that if the particles are pushers, the Nusselt number is increased (i.e., they enhance convective heat transfer) in a simulated natural convection cell. In addition, the pusher swimmers are predicted to cause a dramatic reduction in the suspension viscosity, which is qualitatively consistent with previous rheological studies

mentioned above. In their study, El Hasadi and Crapper theoretically modeled “artificial pushers” that are fabricated from artificial bacterial flagella, which can be driven using an external magnetic field^{27,28}.

Current work

Motivated by the well-known heat transfer enhancement limitations of nanofluids and the promise of self-propelled microparticles, in this work we present molecular dynamics (MD) simulations of self-propelled nanoparticles, and study the effect of the nanoparticles’ motion on thermal transport through the fluid. We find that the nanoparticles’ self-propulsion leads to an overall enhancement of the fluid’s effective thermal conductivity (ETC, defined as the heat transfer rate divided by the average temperature gradient magnitude), as compared to the cases of Brownian (i.e., non-swimming) nanoparticles and of the liquid alone. Suspensions of active particles (especially if they swim as “pushers”) could thus show significantly higher ETC than nanofluids, as well as reduced viscosity. Such fluids would be exceptionally well-suited as heat transfer fluids, since they would enable both higher heat transfer rates and reduced pumping power. The simulations presented here provide a theoretical foundation for this concept and lay the groundwork for future experimental studies. Since we expect that they could be useful in a broad range of heat transfer applications, we suggest the term “active heat transfer fluids” (AHTF) to describe these novel suspensions.

The article is arranged as follows. In section 2 we provide a theoretical description of the problem to be solved and present the details of the MD simulation method we used. Section 3 shows the computational results and discussion. In section 4 we present the major conclusions of the study and discuss directions for future research, as well as the potential practical applications.

2. Simulation Model and Procedure

The nanoparticles were modeled by Lennard-Jones (LJ) atoms carved out of a perfect face-centered-cubic (FCC) crystal. The crystalline atoms forming the nanoparticles are bonded together via FENE (finitely extensible nonlinear elastic) and pairwise Lennard-Jones (LJ) potentials:

$$U_{FENE}(r) = -33.75\epsilon_0 \ln \left[1 - \left(\frac{r}{R_0} \right)^2 \right] + 4\epsilon_0 \left[\left(\frac{\sigma_0}{r} \right)^{12} - \left(\frac{\sigma_0}{r} \right)^6 \right] + \epsilon_0, \quad (1)$$

where r is the separation distance between two solid atoms, ϵ_0 and σ_0 are the characteristic energy and distance for the LJ potential, and R_0 is the cutoff for the bond length. The FENE potential ensures that the atoms form a stable FCC crystal regardless of the temperature or strength of the LJ potential. The nanoparticles consist of 429 solid atoms each, forming an approximately spherical shape with a radius of $\sim 4\sigma_0$. For computational efficiency, the interactions among liquid atoms are represented by a repulsive LJ model,

$$U_{LJ} = 4\epsilon_0 \left[\left(\frac{\sigma_0}{r} \right)^{12} - \left(\frac{\sigma_0}{r} \right)^6 \right] + \epsilon_0, \quad (2)$$

which is truncated at a separation distance of $2^{1/6}\sigma_0$. The mass of each liquid atom is m_0 and the mass of each nanoparticle atom is $3m_0$. The number density of the atoms constituting the nanoparticle is over 2 times larger than that of the liquid. As a result, the nanoparticle density is roughly 6.5 times larger than that of the liquid. Nanoparticle-liquid interactions are mediated by the same forces as liquid-liquid interactions, which are described by equation (2).

For the initial simulations, which focus on quantifying the translational and rotational diffusivity of the nanoparticles, the simulation box contains one nanoparticle; for thermal transport simulations, eight nanoparticles are used. In the case of single-nanoparticle simulations, the number of liquid atoms was varied from 3,125, 6,250 to 12,500 to study the effect of the domain size (Figure 1). For the eight-

nanoparticle system we used a total of 6,250 liquid atoms per nanoparticle, i.e. a total of 50,000 liquid atoms and 3,432 solid/nanoparticle atoms.

Preparation of Samples

The nanoparticle was inserted into a liquid matrix with a preexisting spherical cavity, whose size was defined to avoid overlaps. The combined system was equilibrated for 1 million time steps under a constant pressure and temperature (NPT) ensemble at constant pressure of $5\varepsilon_0/\sigma_0^3$ and temperature of $1.0\varepsilon_0/k_B$, where k_B is the Boltzmann constant. Subsequently, the system was equilibrated for 1 million time steps under the Nose-Hoover constant volume and temperature (NVT) ensemble at $1.0\varepsilon_0/k_B$ temperature. After the system was fully equilibrated, we added forces of the same magnitude (ranging from 0.05 to $0.5\varepsilon_0/\sigma_0$) to each atom of half of the nanoparticle to simulate the generation of propulsive force. The half of the nanoparticle to which the force was applied was predefined before the self-propelling process, and the identities of these atoms were kept unchanged during the simulation. We will refer to the group of atoms with added force as the *self-propelled half* of the nanoparticle in the rest of this paper. To conserve momentum, a balancing force, $F_{liquid} = -\sum F_{propulsion} / N_{liq}$ is applied to every liquid atom, where N_{liq} is the number of liquid atoms in the simulation.

The force applied to each atom was directed along the line connecting the atom with the center of mass (COM) of the nanoparticle. Consequently, the direction of the net (overall) propulsion force is always perpendicular to the imaginary plane separating the propelled and non-propelled halves. The direction vector fluctuates stochastically in 3-D space due to rotational Brownian motion. For pullers, the direction of the net propulsive force pointed from the COM to each atom in the (front-facing) self-propelled half. For pushers, the directions of all forces pointed from each atom in the (rear-facing) self-propelled half to the COM. We found that the dynamic behavior of pullers and pushers is almost the same, and so we only present the results of pullers here. To establish a reference, we also studied the system consisting of a nanoparticle without propulsive forces, which was used to simulate standard Brownian motion.

All simulations were conducted using the LAMMPS MD package^{29,30} using a simulation time step of $0.01\tau_0$, where τ_0 is the reduced time unit:

$$\tau_0 = \sqrt{\frac{m_0\sigma_0^2}{\varepsilon_0}}. \quad (3)$$

Characterization of Dynamics

To characterize the dynamics of self-propelled nanoparticles, translational velocity autocorrelation functions and reorientation times were obtained from 42 million time step NVT simulation runs at a temperature of $1.0\varepsilon_0/k_B$. After discarding the first 22 million time steps, we collected the coordinates and velocities of both the COM of the whole particle and the COM of the propelled half at every 5 timesteps.

To characterize translational diffusion of the particles, we calculated the autocorrelation function of the COM of the whole nanoparticle:

$$\Phi_t(t) = \frac{\langle v_\alpha(0)v_\alpha(t) \rangle}{3}, \quad (4)$$

where $\alpha = x, y, z$ represents the three Cartesian coordinates and we are using Einstein notation (thus summation over the three indices is implied). The triangular brackets indicate an averaging over multiple time origins.

The relaxation time for the autocorrelation function, τ_{eff} , can be calculated by fitting an exponential decay to Φ_t :

$$\Phi_t(t) = \Phi_t(0) \exp\left(-\frac{t}{\tau_{eff}}\right). \quad (5)$$

The particle's effective translational diffusion coefficient D_{eff} can then be obtained from the Green-Kubo relation^{31,32}

$$D_{eff} = \int_0^{\infty} \Phi_t(t) dt \quad (6)$$

To estimate the reorientation time, we calculated the vector $\vec{r}(t)$ pointing from the COM of the self-propelled half of the nanoparticle to the COM of the entire nanoparticle. The autocorrelation function of this vector is determined from

$$\Phi_r(t) = \frac{\langle r_\alpha(0)r_\alpha(t) \rangle}{3}, \quad (7)$$

where again the index α indicates each of the Cartesian coordinate directions and the summation is implied. Again, we can fit an exponential decay to the reorientation autocorrelation function Φ_r ,

$$\Phi_r(t) = \Phi_r(0) \exp\left(-\frac{t}{\tau_R}\right), \quad (8)$$

where τ_R is the characteristic reorientation time.

Characterization of Effective Thermal Conductivity

To determine the effect of the self-propulsion on ETC, we simulated 8 nanoparticles in a box of 50,000 liquid atoms. After the system was well-equilibrated, we employed a direct method to calculate the thermal conductivity, in which a planar heat source and planar heat sink were inserted into the domain with the overall thermostat still enabled. The heat source and sink were placed 1/4 of the box length from opposite edges of the box. In addition, we enforce periodic boundary conditions on the edges of the box. Overall, a temperature gradient is established between the heat source and heat sink; a gradient equal in magnitude but opposite in polarity is also established between the heat source and its nearest edge, and between the heat sink and its nearest edge (see Figure 5).

The velocities of the atoms in the heat source and sink region were increased and decreased, respectively, at a constant rate of $200\varepsilon_0 / \tau_0$. This rate is equal to the overall heat transfer rate through the fluid, \dot{Q} . The temperature profile in the system was then calculated by determining the average kinetic energy of the atoms as a function of position. After the temperature gradient, dT/dz , was stabilized, the effective thermal conductivity, k_{eff} , was determined through Fourier's Law:

$$k_{eff} = -\frac{\dot{Q}}{2A(dT/dz)}. \quad (9)$$

The factor of 2 in the denominator of equation (9) is necessary because the total energy consumption/insertion rate, \dot{Q} , flows evenly on either side of the heat sources/sinks. Accordingly, the net heat transfer rate from the heat source to the heat sink is $\dot{Q}/2$.

3. Results and Discussion

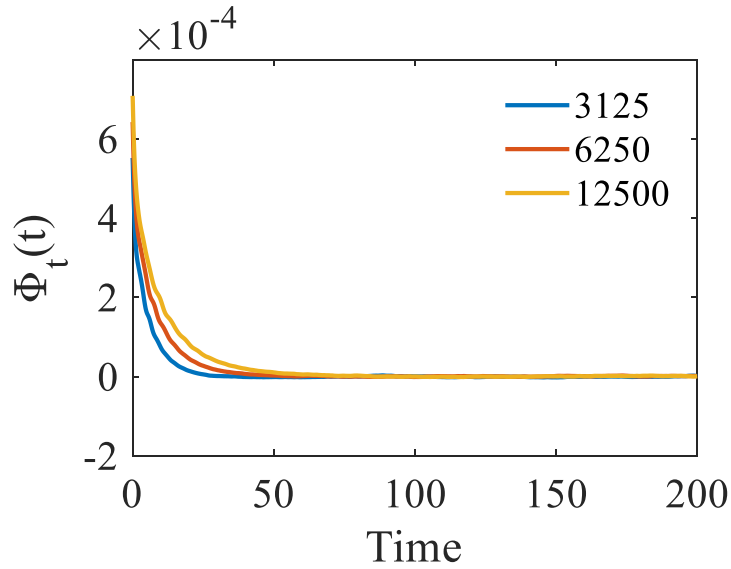


Figure 1: Autocorrelation function of the translational velocity of the center of mass of a nanoparticle undergoing Brownian motion (no self-propulsion) as a function of time (in units of τ_0). The curves of different colors represent systems that contain different numbers of liquid atoms.

To study the effect of system size, we simulated a single Brownian nanoparticle immersed in a box of 3125, 6250, and 12500 liquid atoms. As shown in Figure 1, the autocorrelation function of the center-of-mass (COM) velocity decays at a different rate for systems of different sizes. This size effect is well-documented and understood in the literature within a context of hydrodynamic interactions and momentum conservation³³. We expect the size effect will be reduced if the system contains multiple nanoparticles, as hydrodynamic interactions are screened.

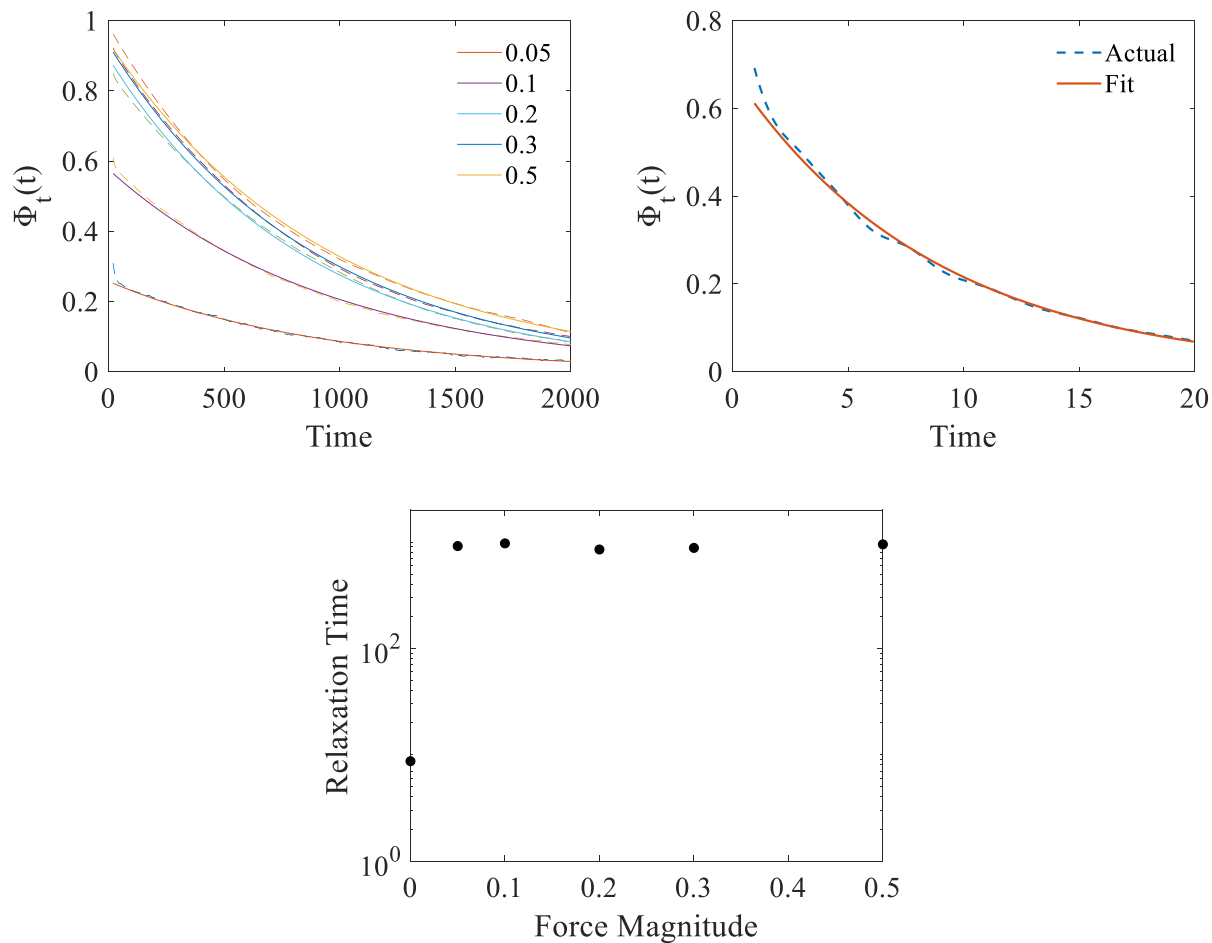


Figure 2: (a) Autocorrelation function of COM velocity for self-propelled nanoparticle with different applied force magnitudes. (b) same as (a), but for a Brownian (non-propelled) nanoparticle. In panels (a) and (b), the exponential fits are plotted as solid curves and the actual values of Φ_{\perp} are plotted as dashed curves. (c) relaxation times of both Brownian (Force magnitude = 0) and self-propelled (Force magnitude > 0) nanoparticles.

The direction of the self-propelled nanoparticles fluctuates stochastically in time due to rotational Brownian motion, which is superimposed on the translational self-propelled motion. Thus, in the absence of an external gradient or magnetic field, the trajectory of artificial microswimmers generally resembles that of an “enhanced random walk” – that is, it resembles Brownian motion but with enhanced effective diffusivity. The dependence of the effective diffusivity of unguided active colloids is well-known to depend quadratically on the self-propelled speed^{16,34}. To verify that the self-propulsion is accurately represented in the MD simulations, here we sought to quantify the effective diffusivity of the self-propelled particles.

To investigate the nature of the diffusion of the self-propelled particles, we studied the autocorrelation function of the COM velocity for self-propelled nanoparticles and compared them with Brownian nanoparticle characteristics. We fitted an exponentially decaying curve to the autocorrelation function to calculate the relaxation time and reorientation time, as described in the previous section and shown in Figure 2a and b. We found that the relaxation times of the self-propelled nanoparticles are significantly longer (by roughly two orders of magnitude) than Brownian nanoparticles. Also, for self-propelled nanoparticles the

relaxation times are independent of the magnitude of the propulsion forces. This suggests two different relaxation mechanisms that we will discuss below.

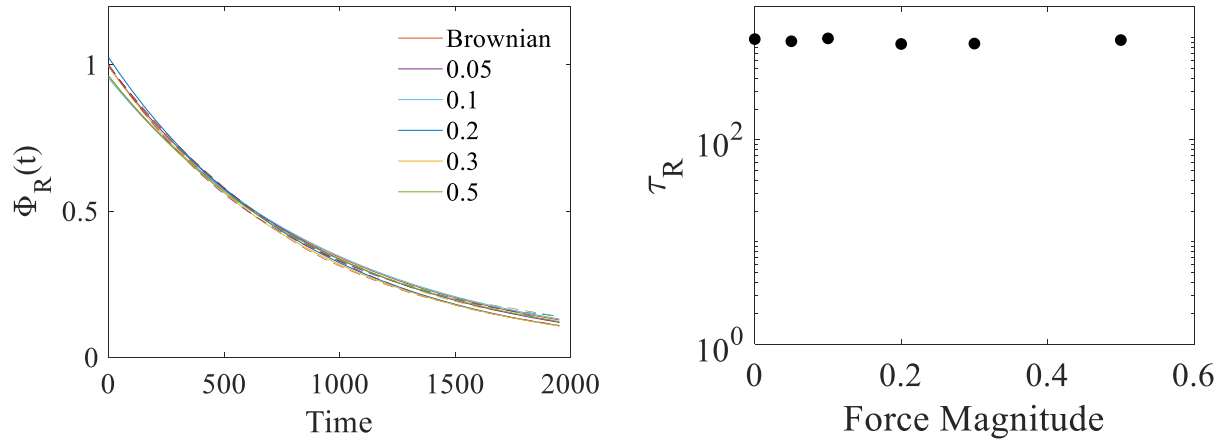


Figure 3: (a) Autocorrelation function of orientation vector for self-propelled and Brownian nanoparticles. The exponential fits are shown as solid curves and the actual values of Φ_R are shown as dashed curves. (b) Corresponding reorientation times as a function of force magnitude.

To understand the different translational velocity relaxation processes and gain further insight into the dynamics of the nanoparticles, we also calculated the orientation vector autocorrelation function and associated reorientation time, as shown in Figure 3. Notably, here the self-propelled and Brownian particles have the same behavior in terms of reorientation and are characterized by the same reorientation time. Furthermore, the reorientation time of self-propelled particles calculated here is the same as the relaxation time of the COM velocity autocorrelation function (see Figure 2). This suggests that the reorientation relaxation mechanism is unchanged after the application of the additional forces, and the application of the forces does not influence the reorientation of particles. This is expected because the directions of the sum of the applied forces were along the COM of the nanoparticle, producing zero torque, which does not affect rotation.

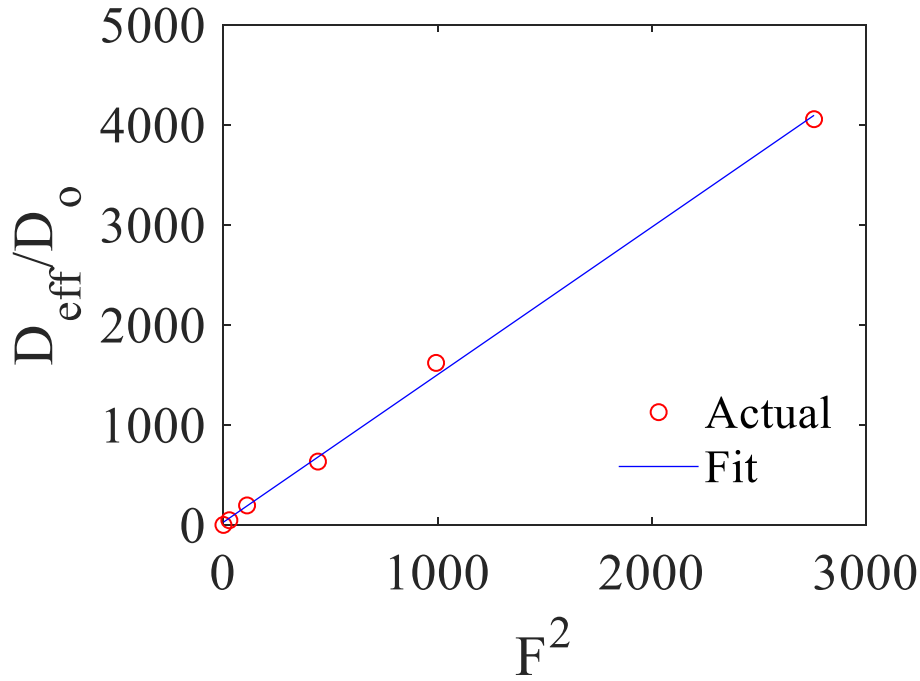


Figure 4: Ratio of self-propelled nanoparticle's effective diffusion coefficient, D_{eff} , to that of the Brownian nanoparticles, D_0 , as a function of propulsive force squared. Red symbols show simulation results, while the blue line indicates a linear least-squares fit.

The above analysis suggests that when the particles propel themselves, the relaxation time for translational motion is dominated by the reorientation relaxation time, as the translational diffusion is dominated by the propulsion velocity, not Brownian velocity. This is illustrated in Figure 4 by plotting the ratio of diffusion coefficients of the self-propelled nanoparticles to the diffusion coefficients of the Brownian nanoparticles, D_{eff}/D_0 . The results in this figure are in the expected range of diffusivity enhancement for self-propelled particles. In previous literature, this ratio has been experimentally observed to be greater than 1000 in many cases³⁴. This ratio is significantly larger than one for all propulsion forces considered in the simulations. Figure 4 suggests a quadratic dependence of D_{eff}/D_0 on F , as demonstrated through the power-law fit to the data:

$$\frac{D_{eff}}{D_0} \approx 1.5F^2. \quad (10)$$

This relation can be understood from the fact that the effective diffusivity of self-propelled nanoparticles is known to be related to the self-propelled speed V_0 by¹⁶

$$D_{eff} = \frac{V_0^2}{6d_r} \quad (11)$$

where $d_r = k_B T / 8\pi\eta R^3$ is the rotational diffusivity of the (spherical) particle, $k_B T$ is the thermal energy, η is the dynamic viscosity of the fluid, and R is the particle radius. From the Stokes drag formula, the velocity is related to the propulsive force magnitude by $F = 6\pi\eta V_0 R$. Combining these relations with equation (11) yields

$$D_{eff} = \frac{RF^2}{27\pi\eta k_B T}. \quad (12)$$

Considering that according to the Stokes-Einstein relationship,

$$D_0 = \frac{k_B T}{6\pi\eta R}, \quad (13)$$

the theoretical estimate predicts the ratio of D_{eff} to D_0 as

$$\frac{D_{eff}}{D_0} = \frac{2}{9} \left(\frac{R}{k_B T} \right)^2 F^2 \approx 3.5F^2, \quad (14)$$

where we have used the fact that, in the MD reduced units system, the thermal energy $k_B T = 1$ and $R \approx 4$. While the prefactor in equation (14) differs from that extracted from the data in Figure 4 (see equation (10)), the coefficient is on the right order of magnitude and the functional dependence on F is the same. This indicates the consistency of the observations based on MD simulations and theoretical propelled and standard Brownian motion analysis.

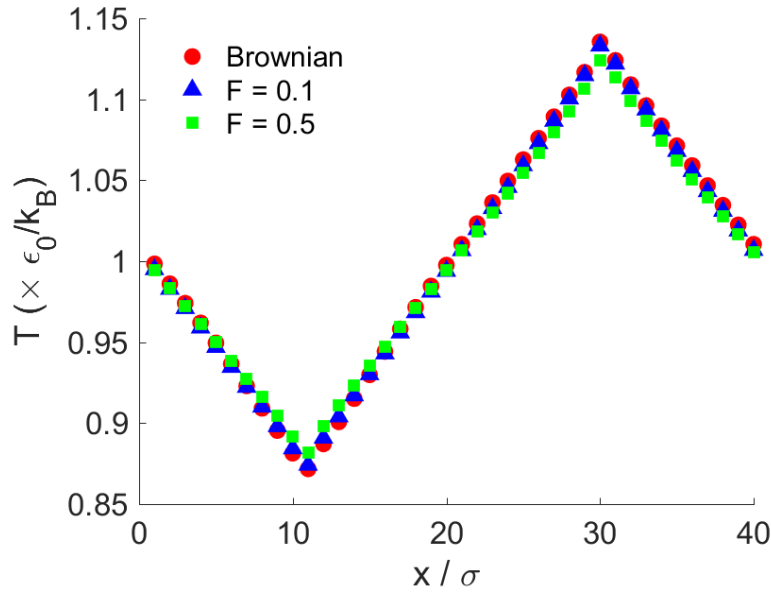


Figure 5: Temperature profile in the simulation box as a function of the magnitude for different propulsive forces when a heat source and heat sink are introduced into the box (the source and sink are inserted at $x/\sigma \approx 30$ and $x/\sigma \approx 10$, respectively).

The analysis of the effective diffusion constant in the case of the propulsion force shows that it can be orders of magnitude larger than that characterizing standard Brownian motion. This suggest that enhanced (propelled) Brownian motion might increase effective thermal conductivity. To test this hypothesis in Fig. 5 we show the steady state temperature profiles for planar heat source-sink simulations of 8 nanoparticle model nanofluids using the same heating/cooling power. The slope of the temperature profile is the highest for the case of Brownian nanoparticles and decreases with increasing propulsion force. Analysis of the data in Figure 5, combined with equation (9), demonstrates a 1.8% increase of (effective) thermal conductivity for an applied force of $0.1\epsilon_0/\sigma_0$ and 8.7% for an applied force of $0.5\epsilon_0/\sigma_0$, as compared to the thermal conductivity of the suspension of Brownian nanoparticles.

4. Summary and Conclusion

We have presented results of MD simulations of self-propelled nanoparticles and studied their effect on the temperature distribution within the fluid. First, we demonstrated that translational and rotational dynamics follow behavior expected from the standard theoretical analysis of standard and self-propelled Brownian nanoparticles. In the case of self-propelled particles, the relaxation time for the translational diffusion coefficient is controlled by the reorientation relaxation time.

As mentioned above, the dynamic behavior of “pushers” and “pullers” was almost the same. This is in contrast to the studies of biological microswimmers mentioned above, in which the qualitative features of pusher and puller suspensions are markedly different. In the present study, it is likely that pushers and pullers show similar results because of the identical spherical shape of both particles, and also their small size (in physical units, the diameter of the nanoparticles considered in this work is on the order of 1-10 nm, which is 3-4 orders of magnitude smaller than the artificial and natural microswimmers considered in most studies). Thus, the hydrodynamic flow fields produced by the pullers and pushers modeled in the present study are not likely to differ substantially from one another, nor do they cause significant disturbances to the background flow. It is possible that the differences between pushers and pullers may be magnified as the particle size is increased. Characterizing the flow fields produced by the swimming nanoparticles, as well as observing the results with larger particles, are both topics for future studies.

In the case of self-propelled nanoparticles (pushers as well as pullers), we observe a discriminable increase of effective thermal conductivity of the fluid. While these increases of up to several percent might be not spectacular, they are significant considering the MD simulations show that without propulsion the nanofluid conductivity is essentially the same as the conductivity of the base fluid. Therefore, our results indicate that self-propelled particles have the potential to enhance thermal conductivity and heat transfer by an amount that can enable new applications in thermal management.

Although the results presented in this paper are promising, it is likely that the enhancement in heat transfer will be increased further with an increase in the particle sizes. The nanoparticles simulated in this work have a diameter equivalent in physical units to a just few nanometers. By contrast, active colloids typically range from 100 nm to 10 μm in size. Thus, the particles simulated here are orders of magnitude smaller than typical active colloids. Heat transfer enhancement is expected to scale with both the size of the active colloids and their self-propelled speed. The exploration of these scaling behaviors will be the subject of future studies.

References

1. Choi, S. U. S. & Eastman, J. A. *Enhancing thermal conductivity of fluids with nanoparticles*. (Argonne National Lab., IL (United States), 1995).
2. Maxwell, J. C. *A treatise on electricity and magnetism*. (Clarendon Press, 1881).
3. Evans, W., Fish, J. & Keblinski, P. Role of Brownian motion hydrodynamics on nanofluid thermal conductivity. *Appl. Phys. Lett.* **88**, 093116 (2006).
4. Babaei, H., Keblinski, P. & Khodadadi, J. M. A proof for insignificant effect of Brownian motion-induced micro-convection on thermal conductivity of nanofluids by utilizing molecular dynamics simulations. *J. Appl. Phys.* **113**, 084302 (2013).

5. Eapen, J. *et al.* Mean-Field Versus Microconvection Effects in Nanofluid Thermal Conduction. *Phys. Rev. Lett.* **99**, 095901 (2007).
6. Putnam, S. A., Cahill, D. G., Braun, P. V., Ge, Z. & Shimmin, R. G. Thermal conductivity of nanoparticle suspensions. *J. Appl. Phys.* **99**, 084308 (2006).
7. Nan, C.-W., Birringer, R., Clarke, D. R. & Gleiter, H. Effective thermal conductivity of particulate composites with interfacial thermal resistance. *J. Appl. Phys.* **81**, 6692–6699 (1997).
8. Buongiorno, J. *et al.* A benchmark study on the thermal conductivity of nanofluids. *J. Appl. Phys.* **106**, 094312 (2009).
9. Lee, T.-C. *et al.* Self-Propelling Nanomotors in the Presence of Strong Brownian Forces. *Nano Lett.* **14**, 2407–2412 (2014).
10. Gao, W., Pei, A. & Wang, J. Water-Driven Micromotors. *ACS Nano* **6**, 8432–8438 (2012).
11. Burdick, J., Laocharoensuk, R., Wheat, P. M., Posner, J. D. & Wang, J. Synthetic Nanomotors in Microchannel Networks: Directional Microchip Motion and Controlled Manipulation of Cargo. *J. Am. Chem. Soc.* **130**, 8164–8165 (2008).
12. Medina-Sánchez, M., Xu, H. & Schmidt, O. G. Micro- and nano-motors: the new generation of drug carriers. *Ther. Deliv.* **9**, 303–316 (2018).
13. Parmar, J., Vilela, D., Villa, K., Wang, J. & Sánchez, S. Micro- and Nanomotors as Active Environmental Microcleaners and Sensors. *J. Am. Chem. Soc.* **140**, 9317–9331 (2018).
14. Mallory, S. A., Valeriani, C. & Cacciuto, A. An Active Approach to Colloidal Self-Assembly. *Annu. Rev. Phys. Chem.* **69**, 59–79 (2018).
15. Chen, X., Zhou, C. & Wang, W. Colloidal Motors 101: A Beginner’s Guide to Colloidal Motor Research. *Chem. – Asian J.* **0**,
16. Saintillan, D. Rheology of Active Fluids. *Annu. Rev. Fluid Mech.* **50**, 563–592 (2018).
17. Guasto, J. S., Johnson, K. A. & Gollub, J. P. Oscillatory Flows Induced by Microorganisms Swimming in Two Dimensions. *Phys. Rev. Lett.* **105**, 168102 (2010).

18. Rafai, S., Jibuti, L. & Peyla, P. Effective Viscosity of Microswimmer Suspensions. *Phys. Rev. Lett.* **104**, 098102 (2010).
19. López, H. M., Gachelin, J., Douarche, C., Auradou, H. & Clément, E. Turning Bacteria Suspensions into Superfluids. *Phys. Rev. Lett.* **115**, 028301 (2015).
20. Wu, X.-L. & Libchaber, A. Particle Diffusion in a Quasi-Two-Dimensional Bacterial Bath. *Phys. Rev. Lett.* **84**, 3017–3020 (2000).
21. Kim, M. J. & Breuer, K. S. Enhanced diffusion due to motile bacteria. *Phys. Fluids* **16**, L78–L81 (2004).
22. Dunkel, J. *et al.* Fluid Dynamics of Bacterial Turbulence. *Phys. Rev. Lett.* **110**, 228102 (2013).
23. Hernandez-Ortiz, J. P., Stoltz, C. G. & Graham, M. D. Transport and Collective Dynamics in Suspensions of Confined Swimming Particles. *Phys. Rev. Lett.* **95**, 204501 (2005).
24. Saintillan, D. & Shelley, M. J. Emergence of coherent structures and large-scale flows in motile suspensions. *J. R. Soc. Interface* **9**, 571–585 (2012).
25. Gregory, D. A. & Ebbens, S. J. Symmetrical Catalytically Active Colloids Collectively Induce Convective Flow. *Langmuir* **34**, 4307–4313 (2018).
26. El Hasadi, Y. M. F. & Crapper, M. Self-propelled nanofluids a path to a highly effective coolant. *Appl. Therm. Eng.* **127**, 857–869 (2017).
27. Ghosh, A. & Fischer, P. Controlled Propulsion of Artificial Magnetic Nanostructured Propellers. *Nano Lett.* **9**, 2243–2245 (2009).
28. Schamel, D. *et al.* Nanopropellers and Their Actuation in Complex Viscoelastic Media. *ACS Nano* **8**, 8794–8801 (2014).
29. Plimpton, S. Fast Parallel Algorithms for Short-Range Molecular Dynamics. *J. Comput. Phys.* **117**, 1–19 (1995).
30. LAMMPS Molecular Dynamics Simulator. Available at: <https://lammmps.sandia.gov/>. (Accessed: 17th May 2019)

31. Green, M. S. Markoff Random Processes and the Statistical Mechanics of Time-Dependent Phenomena. II. Irreversible Processes in Fluids. *J. Chem. Phys.* **22**, 398–413 (1954).
32. Kubo, R. Statistical-Mechanical Theory of Irreversible Processes. I. General Theory and Simple Applications to Magnetic and Conduction Problems. *J. Phys. Soc. Jpn.* **12**, 570–586 (1957).
33. Asta, A. J., Levesque, M., Vuilleumier, R. & Rotenberg, B. Transient hydrodynamic finite-size effects in simulations under periodic boundary conditions. *Phys. Rev. E* **95**, 061301 (2017).
34. Takatori, S. C. & Brady, J. F. Forces, stresses and the (thermo?) dynamics of active matter. *Curr. Opin. Colloid Interface Sci.* **21**, 24–33 (2016).